JOURNAL OF MATERIALS SCIENCE **38** (2003) 1403–1412

Instrumented indentation and ultrasonic velocity techniques for the evaluation of creep cavitation in silicon nitride

F. LOFAJ
Institute of Materials Research of the Slovak Academy of Sciences, 043 53 Košice, Slovakia
E-mail: lofaj@saske.sk

D. T. SMITH, G. V. BLESSING, W. E. LUECKE, S. M. WIEDERHORN
National Institute of Standards and Technology, Gaithersburg, MD 20899, USA

Instrumented indentation and ultrasonic wave velocity techniques combined with precise density change measurements and transmission electron microscopy (TEM) were used to investigate the changes of elastic moduli in silicon nitride after tensile deformation up to 3%. Linear dependencies on strain were also found for the degradation of the indentation modulus, longitudinal and transverse ultrasonic wave velocities, Young's, shear and bulk moduli and Poisson's ratio. The results obtained by indentation technique and ultrasonic method were essentially identical. TEM observation confirmed that multigrain junction cavities were responsible for the density changes and the elastic moduli degradation. The density changes were linearly proportional to tensile strain with the slope of 0.75. Thus, cavitation is the dominant creep mechanism in silicon nitride studied. Instrumented indentation and ultrasound velocity techniques are suitable for non-destructive monitoring of creep damage accumulation in ceramic components.

1. Introduction

Advanced ceramics, particularly silicon nitride, are considered the candidate materials for the components in the high efficiency gas turbines and other structural applications because of their excellent mechanical properties at elevated temperatures. However, the problems with the effects of creep, environment and foreign object damage limit the approval of ceramics for commercial use in gas turbines [1, 2]. Creep and creep damage accumulation are of special interest for determining the lifetime and reliability of the ceramic components during their long-term operation at high temperatures under stress. Numerous creep studies on various grades of silicon nitride pointed out the importance of cavitation during creep in vitreous bonded ceramics [3–9]. Cavities contribute significantly to tensile deformation since their volume is transformed into tensile strain [5–9]. The relationship between the volume fraction of cavities and tensile strain is linear with the slope close to 0.9 in wide range of ceramics [8]. This means that around 90% of total tensile strain results from cavitation. Thus, cavitation was concluded to be the main creep mechanism in silicon nitride and possibly, in other ceramics containing amorphous phase at the grain boundaries [6–9]. The development of cavitation during creep in tension and its suppression in compression are considered to be responsible also for asymmetry in creep behavior [7].

The development of cavities during tensile creep results in gradual change of the density of tested material. Thus, density measurement is the most straightforward method to quantify cavitation. The other methods are based on the influence of porosity on various physical properties of the ceramics, such as ultrasonic velocity, elastic moduli, hardness, etc. Two of them, ultrasonic velocity [10–12] and instrumented indentation [13, 14] are of interest in this work because of their potential application for non-destructive measurement of creep damage accumulation in structural parts from silicon nitride.

The ultrasonic velocity method was applied to wide range of ceramics, [15–25] including silicon nitride [17, 18, 20–22, 24, 25] in order to estimate porosity in these materials. The velocities of the longitudinal waves, v_l, is given by [11, 12]

$$v_l = \{E(1-\upsilon)/(1+\upsilon)(1-2\upsilon)\rho\}^{0.5}, \qquad (1)$$

where the Poisson's ratio, υ, is determined from the shear wave velocity, v_t, and v_l as

$$\upsilon = [1-2(v_t/v_l)^2]/[2-2(v_t/v_l)^2] \qquad (2)$$

Depending on the model of microstructure used for describing the propagation of the ultrasonic waves in porous body, various authors proposed variety of

relationships between Young's modulus and porosity, p [15–23]. However, for small porosities, all relationships can be simplified as

$$E(p) = E_0(1 - b_E p) \tag{3}$$

and

$$v_l = v_{l0}(1 - ap), \tag{4}$$

where E_0 and v_{l0} are the Young's modulus and longitudinal ultrasonic velocity of nonporous material and b_E and a are the corresponding coefficients of proportionality. Because of the linear dependence on porosity, longitudinal velocity alone can be used for non-destructive evaluation of porosity in the components without measuring their density. However, density and velocities of shear and longitudinal wave velocities are necessary for calculation of the absolute values of Young's modulus (see Equation 1).

The number of works using ultrasonic waves for study of deformation in ceramics is considerably more limited because of weak understanding of the relationship between cavitation and strain in these materials in the past. Hasselman *et al.* considered so called "elastic" creep to account for the effect of cracks and cavities on the Young's modulus degradation during creep in early 80's [26, 27]. However, its contribution was insignificant compared to total creep strain. The measurements of Young's modulus changes after bending creep in silicon nitride at that time were highly nonlinear and confusing [28]. In contrast to those results, our recent measurements on silicon nitride subjected to tensile creep produced linear dependence of ultrasonic velocities and elastic moduli on strain and density change [9, 24, 25]. It was concluded that the pulse-echo technique for ultrasonic velocity measurement can be successfully used to monitor cavity accumulation during creep with detection limit for cavitation below 0.5% strain [24, 25]. However, additional density measurements, which are necessary for elastic moduli evaluation besides ultrasonic velocity measurements, are time consuming and non-destructive character of the evaluation is lost.

Instrumented indentation is a fully non-destructive technique when an indentor is pushed into a specimen surface and then withdrawn. The force on the indenter and the penetration depth of the indenter into the specimen are continuously recorded throughout the loading/unloading cycle. The resulting force-displacement curve is then analyzed according to the method of Oliver and Pharr [13] to yield both plastic deformation properties (i.e., hardness) and elastic modulus of the material. Indentation modulus which is given by

$$E_i = E/(1 - \upsilon^2), \tag{5}$$

where E is the Young's modulus, υ is Poisson's ratio, is determined from the slope of the indentation unloading curve under the assumption that the specimen is elastically homogeneous and isotropic. The advantage of indentation method is that absolute values of elastic modulus are obtained without density measurement and the sample can be used for further tests. However, in contrast to the ultrasonic method, the indentation modulus is related to very limited area under the indentor. The method was used in number of experimental studies to investigate the correlation between elastic moduli and porosity or microcracking [29] and even for degradation of elastic moduli during creep and oxidation [30, 31]. Since both E and υ can be obtained from independent ultrasonic velocity and density measurements, the ratio $E/(1 - \upsilon^2)$ calculated from these values can be compared with the indentation modulus, E_i, measured on identical samples.

The objective of the current work is to compare the results of ultrasonic wave velocity technique and instrumented indentation in the study of the elastic moduli degradation in silicon nitride during tensile creep and to determine the role of cavities in creep deformation. An additional goal is to examine the applicability of both methods for the quantification of creep damage accumulation during tensile creep in silicon nitride.

2. Experimental procedure

2.1. Material characterization

The study was carried out on the commercial grade of silicon nitride.* The microstructure of this material has a typical bimodal grain size distribution with a small number of large elongated grains of β-Si_3N_4 randomly distributed in a fine grained β-Si_3N_4 matrix. Secondary phases in the as-received material contain woehlerite, $Yb_4Si_2N_2O_7$ and variable amount of the apatite type H-phase, $Y_5(SiO_4)_3N$, besides small amount of $Yb_2Si_2O_7$ and several unidentified phases. Material composition and mechanical properties of this silicon nitride grade were described elsewhere [7, 9].

2.2. Tensile creep

Tensile creep tests were conducted on dog-bone shaped pin-loaded specimens (type SR 76 [32]). Total length of specimens was 76 mm, the gauge size was 2.5 mm × 2.5 mm × 19 mm. Tensile stresses were applied using single pin SiC pull rods and pneumatic loading system. Creep strain was measured by scanning laser extensometry and two SiC flags attached to the gauge of the specimen [33].

Table I summarizes testing conditions of all specimens included in this study. The samples from thirty two creep tests carried out at temperatures from 1150°C to 1400°C and strains in the range from 0.0004 up to 0.0214 were obtained. Nine new experiments were conducted at 1400°C under stress of 150 MPa. These conditions were chosen because of high reproducibility of the material behavior at this temperature and stress confirmed in an earlier round-robin test [35]. Seven of

*SN 88 (NGK Insulators, Ltd., Nagoya, Japan) Certain commercial equipment, instruments and materials are identified in this paper in order to specify the experimental procedure adequately. Such identification is not intended to imply recommendation or endorsement by the National Institute of Standards and Technology, nor is it intended to imply that the materials or equipment identified are necessarily the best available for the purpose.

TABLE I Summary of the creep conditions, creep performance, ultrasonic velocities and density changes on the samples included in the study

Specimen number	T [°C]	Stress, [MPa]	Time, [h]	Strain, ε	Volume fraction of cavities, f_V	v_l gauge [m/s]	v_l grip [m/s]	v_t gauge [m/s]	v_t grip [m/s]
18A/RR22B[a]	1400	150	0.25	0.0011	0.00037	10356	10376	5775	5778
18A/RR23A[a]	1400	150	2.16	0.0032	0.00239	10391	10386	5802	5811
18A/RR22A[a]	1400	150	5.70	0.0051	0.00281	10363	10410	5834	5808
18A/RR21A[a]	1400	150	24	0.0120	0.00862	10244	10389	5773	5821
20-04 (N2)[a]	1400	150	24	0.0091	0.00834	10290	10373	5811	5812
20-10 (N3)[a]	1400	150	50	0.0018	0.01341	10271	10381	5770	5818
33-25 (N4)[a]	1400	150	69.05b	0.025	0.01772	10185	10357	5734	5784
33-10 (N5)[a]	1400	150	70	00238	0.01652	10173	10392	5723	5820
28-08 (N6)[a]	1400	150	85.06[b]	0.0275	0.01855	10163	10412	5716	5815
04-06	1354	150	616.5	0.0269	0.02144	10198	10451	5751	5833
04-22	1253	250	821.7	0.0142	0.01043	10305	10448	5797	5832
04-26	1250	300	171.3	0.0139	0.01079	10229	10421	5761	5821
04-27	1404	200	8.1	0.0144	0.01039	10296	10428	5782	5816
28-26	1400	150	13.45	0.0066	0.00491	10329	10422	5802	5826
33-21	1400	150	5.02	0.0034	0.00175	10361	10435	5807	5821
12-02	1253	350	12.6	0.008	0.00512	10377	10458	5788	5849
12-04	1154	350	1434	0.0138	0.01085	10293	10447	5758	5832
12-24	1305	300	25.5	0.0121	0.01005	10313	10433	5765	5831
04-10	1152	400	381.9	0.0082	0.00617	10351	10444	5784	5819
12-12	1353	200	98.1	0.0198	0.01598	10227	10416	5756	5819
33-28	1400	20	N/A	0.0073	0.0035	–	–	–	–
33-20	1400	15	N/A	0.0051	0.00313	–	–	–	–
20-27	1350	30	N/A	0.0066	0.00438	–	–	–	–
04-15	1400	150	70.56	0.0229	–	10154	10390	5722	5810
02-01	1400	150	65.01	0.0235	–	10188	10434	5738	5829
34-B01	1400	150	85.01	0.0276	–	10174	10443	5736	5846
88-51-03A	1400	150	45.63	0.0189	–	10176	10405	5742	5817
88-51-11A	1400	150	56.13	0.0241	–	10210	10364	5745	5812
88-51-09B	1400	150	81.63	0.0298	–	10240	10444	5759	5819
88-51-08B	1400	150	33.17	0.0069	–	10285	10432	5775	5839
88-51-11B	1400	150	95.91	0.022	–	10231	10448	5742	5851
20-08	1300	90	6691	0.0276	–	10210	10421	5788	5861

[a]New set of interrupted creep tests; [b]Creep failure at 1400°C under stress of 150 MPa; N/A–not available.

these nine tests were intentionally interrupted at various strains prior to failure and specimens cooled down under load. All other creep experiments lasted until rupture. Twenty three tests were a part of earlier creep studies [34–36].

2.3. Instrumented indentation

Instrumented indentation measurements were made using a nanoindenter* with a three-sided pyramidal diamond Berkovich indenter on a high-load head using a maximum force of 4 N and a loading rate of 0.2 N/s. The samples were cut from the samples after intermittent creep tests at 1400°C and ground to remove oxide layer. Nine computer controlled indentations were made on each of nine gauge-grips pairs of specimens. The same samples were subsequently used for ultrasonic velocity and density measurements. The typical depth of indents was approximately 3 μm and typical contact area was around 200 μm^2. The indentation Young's modulus E_i (see Equation 5) was determined automatically from the slope of the initial part of the unloading cycle of the load-penetration depth curve [13, 14]. The error bars on the reported results represent standard deviation of the average value from nine measurements.

*Model Nano Indenter II, MTS Systems Nano Instruments Innovation Center, USA.

2.4. Ultrasonic velocity measurement

The ultrasonic velocity technique is based on time-of-flight measurements using the pulse-echo technique [12]. Piezoelectric transducers operating at 20 MHz and 10 MHz, driven by shock excitation using a pulser/receiver with a bandwidth frequency of 200 MHz† generated the longitudinal and transverse waves, respectively. Silicone oil and the multipurpose, water-soluble, high-viscosity liquid were used as the ultrasonic couplants between the specimens, delay rod and the corresponding transducer.

Twenty nine gauge-grip pairs of samples for ultrasonic velocity measurements were cut from the gauge and grip areas of the specimens after creep and ground to remove the oxide layers. The size of the bars after grinding was approximately 2.3 mm × 1.7 mm × 10 mm. The transit time, τ_x, ($x = 1$ for longitudinal waves and $x = t$ for transverse or shear waves) for a wave round trip between multiple echoes of the primary signal was measured by digital oscilloscope. Measurements were made at least in two different locations in both transverse directions perpendicular to the tensile stress—across the width and across the thickness of the gauge. Average value of the measurements was used as the representative transit time. The specimen thickness, d, was determined using a digital micrometer with an accuracy of ± 2 μm. The ultrasonic velocity

† Model 5900 PR, Panametrics, USA.

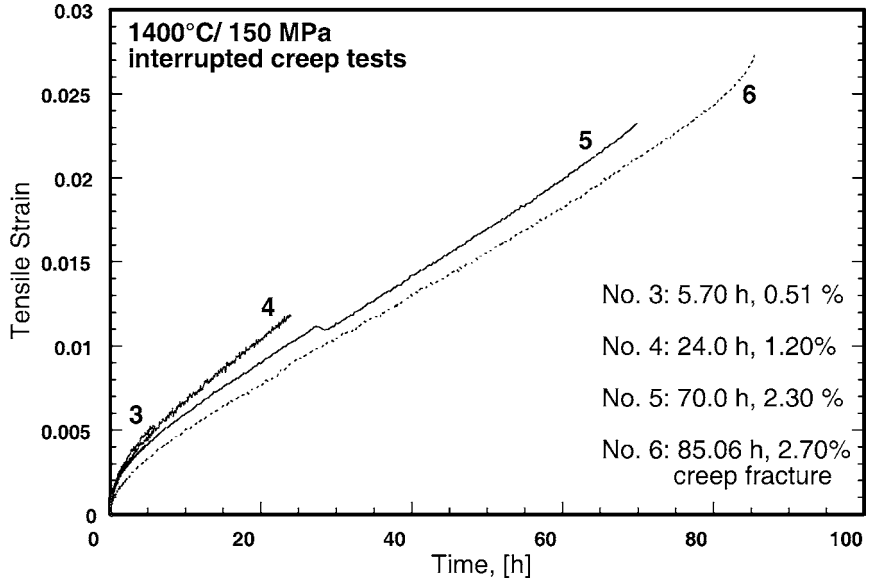

Figure 1 Several tensile creep curves from SN 88 silicon nitride at 1400°C under stress of 150 MPa. The tests No. 1–No. 5 were intentionally interrupted, test No. 6 run until failure.

of the corresponding waves was calculated from $v_x = 2d/\tau_x$.

The relative sound velocity change was determined as a difference between the velocities in the gauge and corresponding velocity in an undeformed grip, v_{x0}, as:

$$\Delta v_x/v_{x0} = (v_x - v_{x0})/v_{x0}, \tag{6}$$

where $x = l$ or $x = t$, respectively.

The Young's modulus was calculated from the Equation 1 with the substitution of Poisson's ratio from Equation 2. The shear modulus, G, and bulk modulus, K, were determined according to the well known relationships [12]

$$G = v_t^2\,\rho \tag{7}$$

$$K = E/3(1 - 2\,\upsilon) \tag{8}$$

2.5. Density measurement

The sink-float technique was used for the measurement of the density in twenty three gauge-grip pairs. Most of the pairs were already used for ultrasonic velocity measurements. They were put into a water solution of thallium malonate formate in a borosilicate glass-jacketed tube connected to the constant temperature water recirculator. The density of solution was adjusted by adding small amount of distilled water at room temperature in such a way that the heaviest specimen started to sink. The temperature coefficient of the density solution was calibrated using two floats of known density certified to ± 0.0005 g/cm^3.* By adjusting the temperature of the solution with water recirculator, it was possible to bracket the buoyancy temperature of each specimen with the accuracy better than 0.5°C. Knowing the temperature coefficient of the density change of the solution, the density of the specimens was calculated from the measured buoyancy temperature. The repeatability of the density measurements was approximately ± 0.00135 g/cm^3. Relative density change, which is equivalent to the volume fraction of cavities, f_v, was determined as a difference between the densities of the deformed sample from the gauge, ρ_{gauge}, and undeformed grip sample, ρ_{grip},

$$f_v = \Delta\rho/\rho_{\text{grip}} = (\rho_{\text{grip}} - \rho_{\text{gauge}})/\rho_{\text{grip}}.$$

2.6. TEM study

The samples for the transmission electron microscopy (TEM) studies were cut parallel to the direction of the applied stress from the gauge specimens used for ultrasonic and density measurements. After four step hand grinding and polishing to $\sim$100 μm thickness and dimpling, the foils were thinned until foil perforation by ion milling at 5 kV. Transmission electron microscopy investigations on carbon coated specimens at 200 kV† were carried out to confirm the presence and to investigate the type of cavities formed during creep.

3. Results

Creep curves obtained from the interrupted creep tests at 1400°C are illustrated in Fig. 1. Three tests (No. 1–No. 3) were interrupted during primary stage of creep, fourth and fifth tests during steady state-like stage and the last test (No. 6) run until failure. The curves from different specimens and tests are close to each other. Small differences between them may result from small variations in material composition among different batches and in alignment of the specimens in the loading train. Reproducibility of creep behavior is important for obtaining consistent strain dependence from the measurements on different samples.

*R.P. Cargille Laboratories, Cedar Groove, NJ.

†EM 300, Philips, The Netherlands

The absolute values of the indentation moduli are summarized in Table II and plotted in dependence on strain for nine interrupted creep tests in Fig. 2. The values of the moduli in the grips are approximately constant and its average value is 321.1 ± 3.9 GPa. The moduli in the gauges decrease with strain.

The velocities of the longitudinal and shear wave were measured on the same samples and from another twenty pairs of samples from the earlier creep experiments (see Table I). The results are shown in Figs 3 and 4. Open symbols in the plots are related to new interrupted experiments and the full symbols to the old creep

TABLE II The comparison of the indentation moduli obtained from instrumented indentation with the moduli calculated from the ultrasonic velocities and density

Sample	Strain, ε	Porosity, f_V	Indentation modulus, E_i, gauge	Indentation modulus, E_i, grip	Calculated $E/(1-\upsilon^2)$ gauge	Calculated $E/(1-\upsilon^2)$ grip
18A/RR22B	0.0011	0.00037	314.36 ± 1.45	318.85 ± 3.19	325.88	326.74
18A/RR23A	0.0032	0.00239	319.00 ± 1.02	323.12 ± 2.87	328.33	329.51
18A/RR22A	0.0051	0.00281	316.08 ± 4.24	317.53 ± 1.66	328.84	329.64
18A/RR21A	0.0120	0.00862	304.50 ± 2.16[a]	305.24 ± 1.91[a]	320.24	330.19
20-04	0.0091	0.00834	311.98 ± 2.22	321.41 ± 3.08	320.62	325.78
20-10	0.0018	0.01341	313.34 ± 3.33	327.52 ± 2.33	296.68	304.61
33-25	0.0250	0.01772	312.00 ± 2.66	324.89 ± 1.96	313.18	326.80
33-10	00238	0.01652	304.52 ± 2.56	315.66 ± 2.23	311.92	329.36
28-08	0.0275	0.01855	299.87 ± 2.23	320.07 ± 2.67	311.08	330.20

[a]These data deviate significantly, possibly because of local defect and therefore, they were not considered in the calculation of the fit.

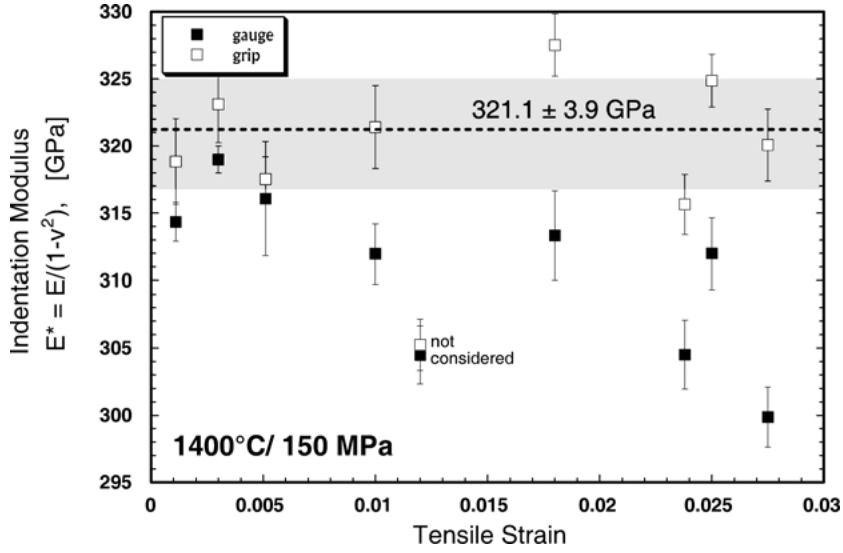

Figure 2 Strain dependence of the absolute values of indentation modulus in the grips and gauges.

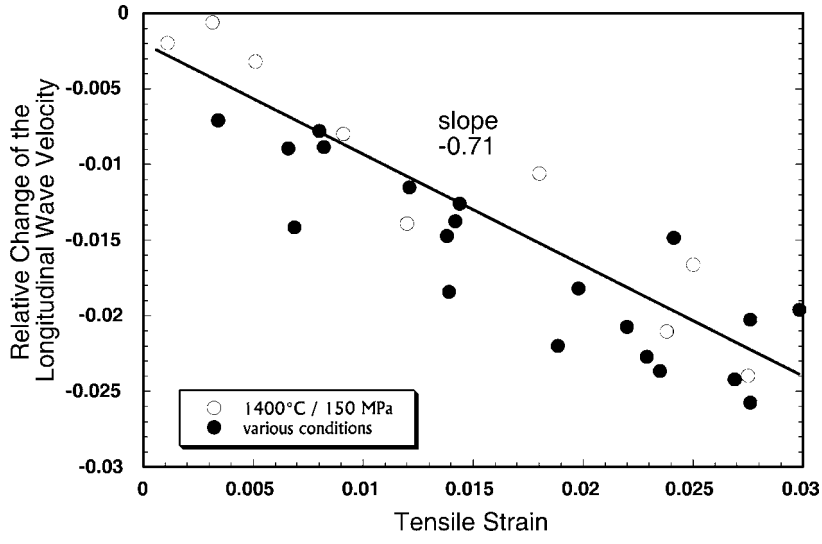

Figure 3 Strain dependence of the relative change of the longitudinal waves. Open symbols correspond to new interrupted tests at 1400°C under stress of 150 MPa, full symbols to the earlier creep tests.

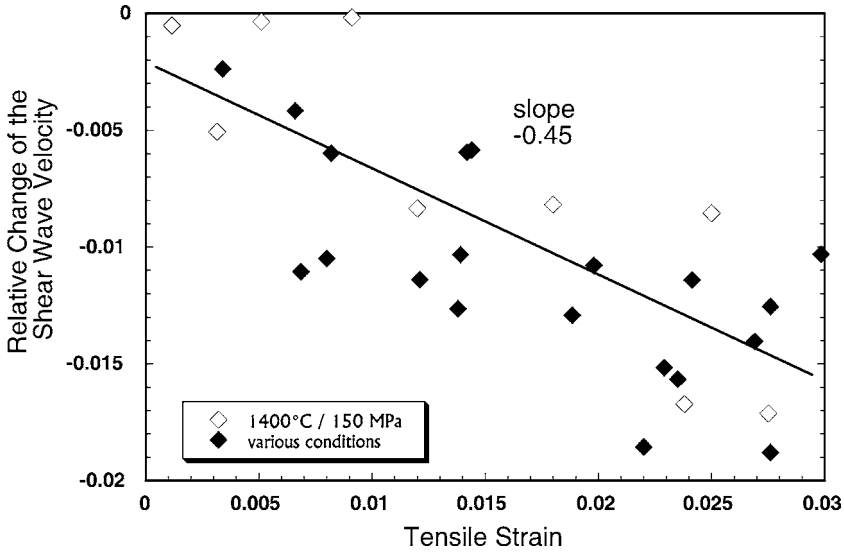

Figure 4 Dependence of the relative velocity change of the shear waves on creep strain.

tests. Longitudinal and shear wave velocities in different grips were approximately constant regardless of the annealing history similarly as in the case of indentation moduli. Their average values were 10 416 ± 29 m/s and 5823 ± 17 m/s, respectively. The velocities in the gauges also decreased with strain. The data fit linear dependence on strain in agreement with the Equation 4. The slopes of 0.61 and 0.79 were found for longitudinal waves in the case of new interrupted tests and old creep experiments, respectively. The slope of the fit of the full data set was 0.71 (Table III). The corresponding slopes for shear waves are 0.36 and 0.56 with the value of 0.45 for the full data set. Note that the data from all tests follow the same dependence regardless of the temperature, stress and strain even in the case of interrupted tests. Strain dependence of the Poisson's ratio is shown in Fig. 5. Significant scatter of the data reduces the reliability of the fit. Assuming linear dependence on strain, the slope is 0.62.

The relationships between relative density change (volume fraction of cavities, f_v) and strain, as well as the strain dependencies of the relative elastic moduli, which were calculated from the known densities and corresponding ultrasonic velocities according to Equation 1 and Equations 4 to 5, are shown in Fig. 6. The meaning of the open and full symbols is identical to that in Figs 3 and 4. Volume fraction of cavities is proportional to tensile strain as described as

$$f_v = k_\rho(\varepsilon - \varepsilon_{th}), \tag{9}$$

where ε_{th} is a threshold strain and k_ρ is the coefficient of proportionality. The values of k_ρ are approximately 0.69 for interrupted tests and 0.85 for old creep tests performed at various conditions. The coefficient of proportionality for all data set is 0.75 (see Table III). Threshold strain is approximately 0.005. The absolute and relative values of the calculated Young's, shear and bulk moduli

TABLE III The comparison of the coefficients of proportionality of ultrasonic velocities, densities and elastic moduli on strain and volume fraction of cavities obtained in the current work and those reported in literature

	Strain dependence; coefficient of proportionality	Porosity dependence; coefficient of proportionality	Literature value for porosity dependence/ (95% confidence interval)
$\Delta v_l/v_{l0}$	0.712 $R = 0.8839$	1.034 $R = 0.9209$	1.34,[22] 1.04,[24] 1.41 (1.34–1.48) [22] 1.15 (0.86–1.44) [21] 1.27 (1.15–1.40) [21–22]
$\Delta v_t/v_{t0}$	0.453 $R = 0.7718$	0.653 $R = 0.7749$	1.18 (1.06–1.30),[22] 1.10 (0.58–1.62),[21] 1.07 (0.93–1.22),[21–22] 0.66,[24]
$\Delta v/v_0$	0.623 $R = 0.6432$	0.900 $R = 0.6119$	—
$\Delta\rho/\rho_0$	0.753 $R = 0.9875$	–	0.69,[25] ∼0.90,[7,9] 1.02 ± 0.03,[36] 0.93 ± 0.04,[6] 0.8–1,[4–5,8]
$\Delta E/E_0$	1.875 $R = 0.9444$	2.492 $R = 0.9404$	1.74,[17] 3.11,[17,a] 2.39/−2.32,[17,b] 2.36/−2.82,[17,c] 2.00–3.03,[18] 2.44,[24] 2.00–3.03,[18]
$\Delta G/G_0$	−1.710 $R = 0.9150$	−2.265 $R = 0.9080$	2.27,[17] 2.0,[20]
$\Delta K/K_0$	−2.585 $R = 0.9332$	−3.484 $R = 0.9419$	-

[a]$Y_2O_3 + SiO_2$ doped, porosity up to 12%; [b]CeO_2 doped porosity <38% and <13%, respectively; [c]MgO doped, porosity <44% and <0.13%, respectively.

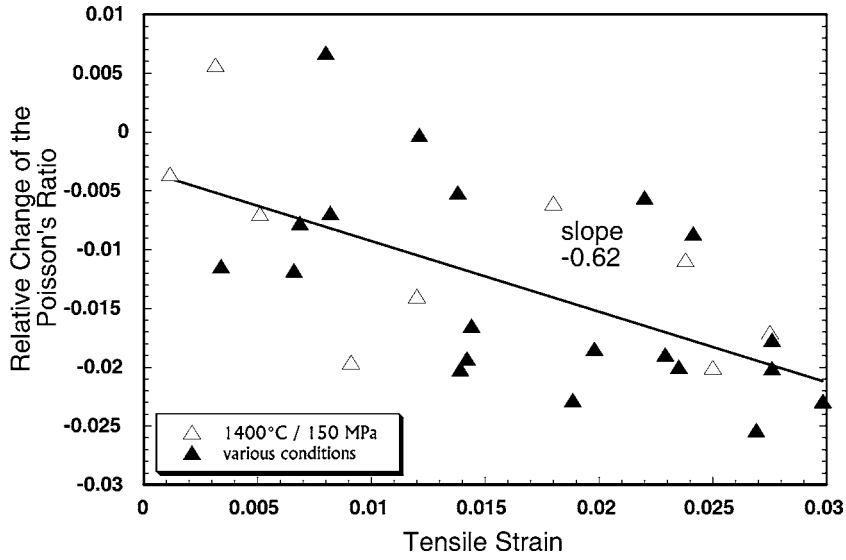

Figure 5 Poisson's ratio dependence on strain in SN 88. Large scatter of the data limits the reliability of the linear fit.

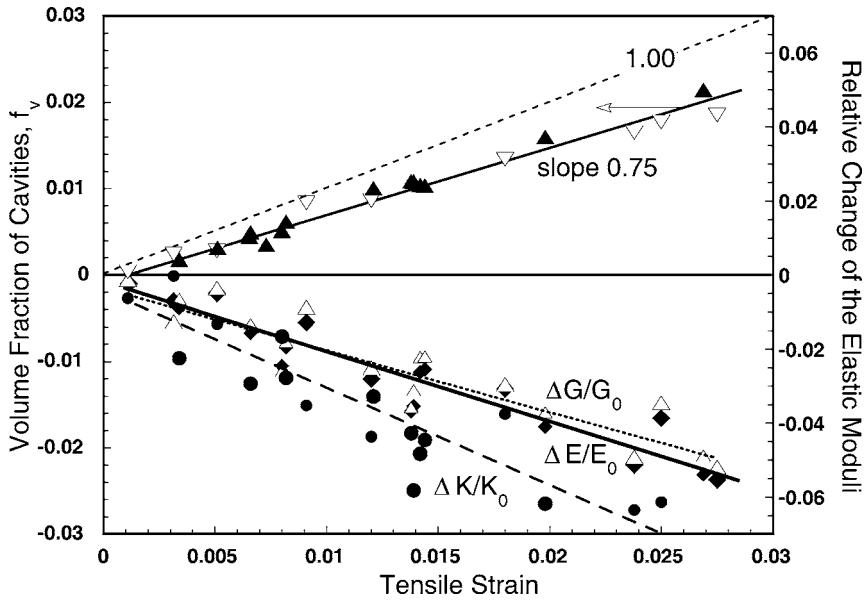

Figure 6 Summary of the density and elastic moduli dependencies on strain. Linear increase in density change results in linear degradation of the Young's modulus, shear modulus and bulk modulus.

linearly decrease with strain (Fig. 6). The corresponding coefficients of proportionality are summarized in Table III.

Fig. 7 is a comparison of the relative indentation moduli and equivalent ratio calculated from ultrasonic velocity and density data from gauges and grips. The decrease of the relative moduli in both cases follows linear dependence with the slope of the fit of 1.67 and 2.0, respectively.

Fig. 8 is a small magnification TEM micrograph of the microstructure of the samples after creep deformation. Creep cavities were the most common type of defects observed. All of them were the multigrain junction cavities with geometry varying from wedge-shaped cavity to irregular full-facet size cavities. Their size was in the range from several nanometers up to approximately 500 nm. The mean size of the cavities estimated from a multiple observations was in the range from 300 nm to 400 nm. The other types of cavities and creep defects, which were reported after long-term creep tests in similar material [37], were not observed.

4. Discussion

The TEM study suggests that cavitation at multigrain junctions is responsible for the change in density. The increase of the volume fraction of such cavities with strain is equivalent to gradual increase of porosity, which may subsequently result in degradation of the ultrasonic velocities, elastic moduli and indentation modulus similarly as in the materials sintered with different levels of porosity studied earlier [11–18]. Thus, tensile deformation is, in limited sense, opposite to the process of sintering.

The physical meaning of the linear change of density with strain (Equation 10) is that cavities accumulate starting from small threshold strains and that around

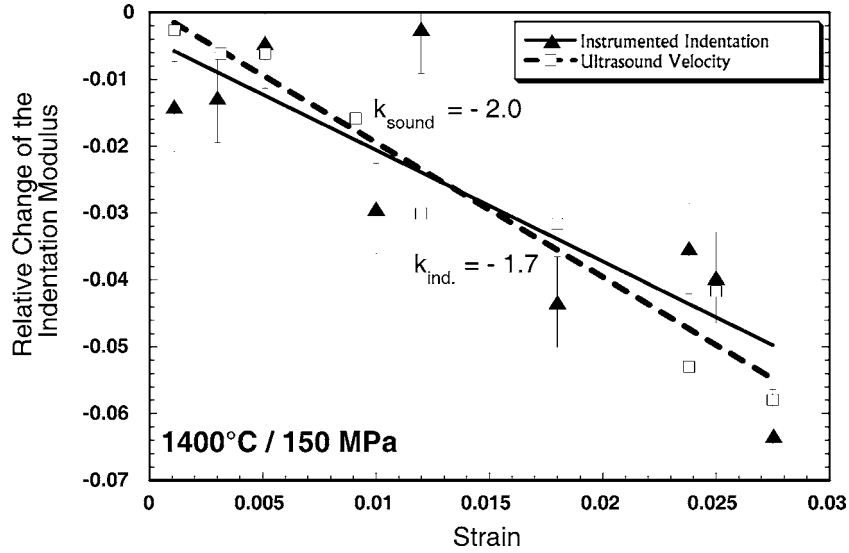

Figure 7 A comparison of the relative change of the indentation modulus E_i and corresponding modulus $E/(1-\upsilon^2)$, which was calculated from the known densities and ultrasonic wave velocities, on strain.

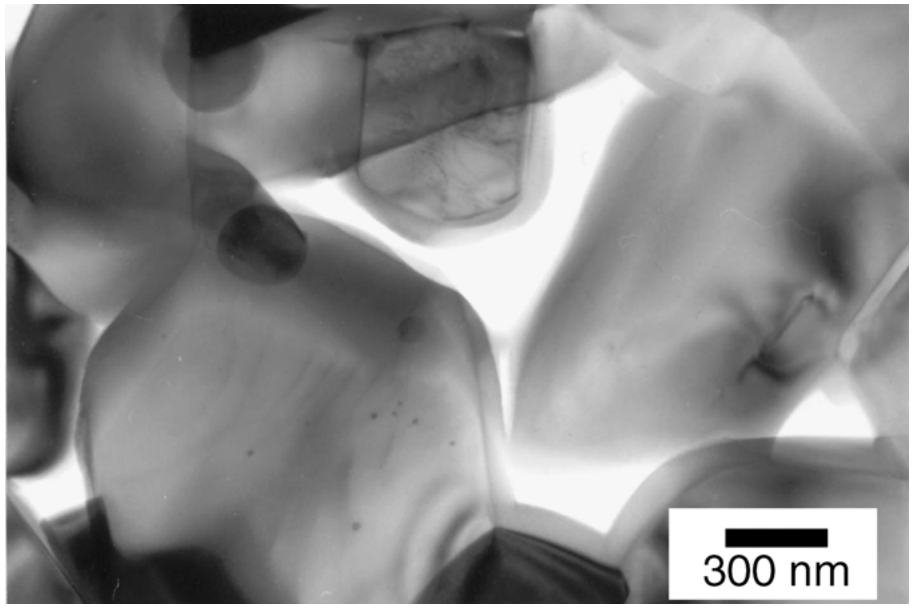

Figure 8 TEM micrograph of the microstructure of silicon nitride studied after tensile creep deformation at 1400°C indicates the presence of the multigrain junction cavities.

75% of the tensile strain results from cavitation. It suggests that cavitation is the dominant creep mechanism in silicon nitride studied. This is in full agreement with our earlier conclusions for this type of materials [6–9, 25, 31, 35, 36]. Another consequence is that the corresponding mechanism has to generate cavities continuously during deformation, even during primary and late stage of deformation, to obey linearity. Possible creep processes necessary for continuous cavitation considered include grain boundary sliding, viscous flow and solution-precipitation [9]. A cavitation creep model based on the existence of dilatational stresses and identical mechanisms has been developed by Luecke and Wiederhorn [5]. Creep behavior of the current material is fully consistent with this model [36]. The existence of small threshold strain and up to 25% of strain unrelated to cavitation indicate the existence and contribution of the volume-conservative creep mechanisms operating simultaneously with cavitation. The ratio between these two kinds of mechanisms can vary from almost unity to zero depending on the chemistry and properties of the secondary phases [38].

4.1. Instrumented indentation vs. ultrasonic velocity technique

The indentation modulus from nanoindentation can be compared with the equivalent parameter $E/(1-\upsilon^2)$ calculated from the known Young's modulus and Poisson's ratio. The average $E/(1-\upsilon^2)$ in the grips is 325.9 ± 8.1 GPa, which is effectively equal to 321.1 ± 3.9 GPa determined from indentation tests (see Table II). Fig. 7 illustrates not only the strain dependence of the relative indentation modulus but also that of the calculated modulus. The results of both techniques can be described by linear fits with the slopes of 1.67 and 2.0. Despite this difference, the data from both methods principally overlap and the slope difference is within

the confidence limit of a fit of instrumented indentation data. Thus, both methods provide almost identical results.

Elastic moduli determined by ultrasonic method represent an average value from the volume of the whole sample, that is around 40 mm^3. However, indentation modulus is obtained only from the volume below the indentation impression, which is around 200 $\mu m^2 \times 10\ \mu m = 2 \times 10^{-6}\ mm^3$. Despite seven orders of magnitude difference in the affected volume, results are very similar. Such agreement can be explained when the density of cavities is considered.

The mean grain size of the silicon nitride grains in the material studied is around 0.8 $\mu m \times 0.8\ \mu m \times 2.5\ \mu m$. It contains approximately 10 vol% of the secondary phases distributed homogeneously in the multigrain junctions. The secondary phase pocket size is assumed to be 0.4 $\mu m \times$ 0.4 $\mu m \times 0.4\ \mu m$ (see Fig. 8). Then, the volume of 2000 μm^3 affected by indentation would be a cube with the sides corresponding to 10–11 grain diameters. It contains ~1125 silicon nitride grains and approximately 3125 secondary phase pockets, that is almost three pockets at each silicon nitride grain. According to cavitation creep model [5], cavities form via redistribution of the secondary phase among the multigrain junctions. Then, the strain of 1% would result in 0.75% increase of total volume of material due to cavitation (see Equation 9). This requires formation of ~235 full pocket size cavities. It means that one of ~13 secondary phase pockets would cavitate or one cavity would be surrounded by 5 silicon nitride grains. Linear dimensions of the remaining pockets would increase to 0.412 μm, that is only by ~3% due to redistribution of the material from the cavitated pockets. The average volume of ~8.6 μm^3 of material per one cavity is considerably smaller than the volume of ~2000 μm^3 affected during indentation. Thus, the effect of each cavity on elastic modulus can be averaged over sufficient number of cavities, silicon nitride grains and remaining secondary phase pockets. The indentation moduli data are therefore representative and identical to those obtained from considerably larger volume affected during ultrasonic velocity measurements.

4.2. Tensile strain and cavitation vs. elastic moduli

Equation 9 also provides a relationship between the strain and porosity dependence of the elastic moduli. For $f_v = p$, substitution into Equation 3 results in

$$E/E_0 = (1 - b_E f_v) = (1 + b_E k_\rho \varepsilon_{th} - b_E k_\rho \varepsilon). \quad (10)$$

Thus, $b_E k_\rho$ corresponds to the coefficient of proportionality of strain dependence of 1.87 in Table III. The coefficients for strain dependence of shear modulus, $b_G k_\rho = 1.71$, and bulk modulus, $b_K k_\rho = 2.58$, were obtained in similar way. Equation 10 points to the differences between strain and porosity dependence of the elastic moduli (Equation 3). They result not only from different coefficient of proportionality but also from the presence of small threshold strain for cavitation. There is no physical reason for change in elastic moduli at small strains ($\varepsilon < \varepsilon_{th}$) at the very early stage of deformation resulting from non-cavitation mechanisms. Because of ε_{th}, the coefficients b_E of strain dependence should be slightly higher compared to those reported for porosity dependence of the elastic moduli. However, the shift from the unity is considerably smaller (0.009 for $b_E = 2.5$, k_ρ and $\varepsilon_{th} = 0.005$) than the scatter of the experimental data and it can be neglected. Then, it can be assumed that $b_E k_\rho = k_E$ or that the contribution of cavitation in tensile strain, which is determined by the coefficient k_ρ, is given by the ratio between coefficients k_E and b_E

$$k_\rho = k_E / b_E \quad (11)$$

Similar equations can be derived for the porosity dependence of the shear and bulk moduli and k_ρ can be determined from the ratios k_G/b_G and k_K/b_K as well. Equation 11 could be eventually used as a method for easy identification of the cavitation creep mechanism without density measurement if b_E and k_E are obtained independently.

The corresponding coefficients k_E, k_G and k_K are summarized in Table III simultaneously with the calculated coefficients of b_E, b_G, and b_K. These coefficients are compared with the coefficients reported by various authors for Young's modulus degradation in silicon nitrides with controlled porosity. Obviously, the measured coefficients agree reasonably well with those reported in silicon nitrides with different porosity levels. The deviations can be related not only to the effect of non-cavitation creep mechanisms but also to the differences in composition, microstructure and measuring techniques. Thus, porosity originating from cavitation during deformation and porosity due to incomplete densification have an identical effect on the degradation of elastic moduli revealed by ultrasonic and indentation methods. Both methods can be used for the monitoring the evolution of cavities in silicon nitride during tensile deformation.

5. Conclusions

Instrumented indentation and ultrasonic wave velocity techniques combined with precise density measurements and TEM were used to investigate the effect of tensile deformation up to 2.7% on elastic moduli in silicon nitride. The changes of the density were linearly proportional to tensile strain with the slope of 0.75. Linear dependencies on strain and volume fraction of cavities (porosity) were also found for the degradation of the indentation modulus, longitudinal and transverse ultrasonic wave velocities, Young's modulus, shear and bulk moduli and Poisson's ratio. TEM observation confirmed that multigrain junction cavities were responsible for the density changes and degradation of the elastic properties. The results obtained by indentation technique and ultrasonic method were essentially identical. This is possible because the indentation affected volume contains sufficient number of cavities to modify the measured physical properties.

Cavitation was concluded to be the dominant creep mechanism in silicon nitride studied. Instrumented indentation and ultrasound velocity techniques are suitable for non-destructive monitoring of the accumulation of creep cavities in ceramic components.

Acknowledgment

The support for the stay of F. Lofaj at NIST provided by Fulbright Commission and NIST is gratefully acknowledged. The work was partially supported by VEGA Grant No. 2/7011/20.

References

1. M. YOSHIDA, K. TANAKA, S. TSURUZONO and T. TATSUMI, *Industrial Ceramics* **19** (1999) 188.
2. M. VAN ROODE, J. R. PRICE, O. JIMENEZ, N. MIRIYALA and S. GATES JR, in "Proc. 7th Int. Symp. Ceramic Materials & Components for Engines," edited by J. G. Heinrich and F. Aldinger (Willey-VCH, Weinheim, Germany, 2001) p. 261.
3. M. N. MENNON, H. T. FANG, D. C. WU, M. G. JENKINS, M. K. FERBER, K. L. MOORE, C. R. HUBBARD and T. A. NOLAN, *J. Amer. Ceram. Soc.* **77**(5) (1994) 1217.
4. C. J. GASDASKA, *ibid.* **77**(8) (1994) 2408.
5. W. E. LUECKE and S. M. WIEDERHORN, *ibid.* **82**(10) (1999) 2769.
6. W. E. LUECKE, S. M. WIEDERHORN, B. J. HOCKEY, R. E. KRAUSE JR. and G. G. LONG, *ibid.* **78**(8) (1995) 2085.
7. F. LOFAJ, A. OKADA and H. KAWAMOTO, *ibid.* **80**(6) (1997) 1619.
8. S. M. WIEDERHORN, B. J. HOCKEY and W. E. LUECKE, *ibid.* **19** (1999) 2273.
9. F. LOFAJ, *Mater. Sci. Eng.* A **279**(1/2) (2000) 61.
10. Z. HASHIN, *J. Appl. Mech., Trans. ASME*, **29**(1) (1962) 143.
11. G. V. BLESSING, in ASTM STP 1045, "Dynamic Elastic Modulus Measurements in Materials," edited by A. Wolfenden (ASTM, Philadelphia, PA, 1990) p. 47.
12. "Standard Practice for Measuring Ultrasonic Velocity in Materials," ASTM E 494-95, Vol. 03.03 (ASTM, Philadelphia, PA, 1995) p. 185.
13. W. C. OLIVER and G. M. PHARR, *J. Mater. Res.* **7**(6) (1992) 1564.
14. K. ZHENG. and C.-H. CHIU, *Acta Mater.* **49** (2001) 353.
15. R. M. SPRIGGS, *J. Amer. Ceram. Soc.* **44**(12) (1961) 628.
16. E. A. DEAN and J. A. LOPEZ, *ibid.* **66**(5) (1983) 366.
17. K. K. PHANI and S. K. NIYOGI, *J. Mater. Sci. Lett.* **6** (1987) 511.
18. S. K. DATTA, A. K. MUKHOPADHYAY and D. CHAKRABORTY, *Amer. Ceram. Soc. Bull.* **68** (1989) 2098.
19. M. KUPKOVA, *J. Mater. Sci.* **28**(19) (1993) 5265.
20. W. A. FATE, *J. Amer. Ceram. Soc.* **57**(8) (1974) 372.
21. J. S. THORP and T. G. BUSHELL, *J. Mater. Sci.* **20**(6) (1985) 2265.
22. D. J ROTH, D. B. STANG, S. M. SWICKARD, M. R. DEGUIRE and L. E. DOLHERT, *Materials Eval.* **49** (1990) 883.
23. J. P. PANAKKAL, *ibid.* **56** (1997) 1367.
24. J.-W. CAO, F. LOFAJ and A. OKADA, *J. Mater. Sci.* **36,** (2001) 1301.
25. F. LOFAJ, G. V. BLESSING and S. M. WIEDERHORN, *J. Amer. Ceram. Soc.*, to be published.
26. D. P. H. HASSELMAN and A. VENKATESWARAN, *J. Mater. Sci.* **18** (1983) 161.
27. D. P. H. HASSELMAN and A. VENKATESWARAN, in "Deformation of Ceramic Materials II," edited by R. E. Tressler and R. C. Bradt (Plenum Press, New York, USA, 1984) p. 525.
28. G. GRATHWOHL, in "Deformation of Ceramic Materials II," edited by R. E. Tressler and R. C. Bradt (Plenum Press, New York, USA, 1984) p. 573.
29. D. T. SMITH and L. H. WEI, *J. Amer. Ceram. Soc.* **78**(5) (1995) 1301.
30. F. LOFAJ, A. OKADA, Y. IKEDA, Y. MIZUTA, H. USAMI and H. KAWAMOTO, *Key Eng. Materials,* **175/176** (2000) 321.
31. A. OKADA and F. LOFAJ, *J. Eur. Ceram. Soc.,* **20**(10) (2000) 1521.
32. J. D. FRENCH and S. M. WIEDERHORN, *J. Amer. Ceram. Soc.*, **79**(2) (1996) 550.
33. W. E. LUECKE and J. D. FRENCH, *ibid.* **79**(6) (1996) 16.
34. R. F. KRAUSE, JR., W. E. LUECKE, J. D. FRENCH, B. J. HOCKEY and S. M. WIEDERHORN, *ibid.* **82**(5) (1999) 1233.
35. W. E. LUECKE and S. M. WIEDERHORN, *ibid.* **80**(4) (1997) 831.
36. K. J. YOON, S. M. WIEDERHORN and W. E. LUECKE, *ibid.* **83**(8) (2000) 2017.
37. F. LOFAJ, H. USAMI, A. OKADA and H. KAWAMOTO, *ibid.* **82**(4) (1999) 1009.
38. F. LOFAJ, S. M. WIEDERHORN, G. G. LONG, B. J. HOCKEY, P. R. JEMIAN, L. BROWDER, J. ANDREASON and U. TÄFFNER, *J. Eur. Ceram. Soc.* **22**(14/15) (2002) 2479.

Received 29 May
and accepted 16 December 2002